Increased Sensitivity of Amino-Arm Truncated βA3-Crystallin to UV-Light–Induced Photoaggregation

Yuri V. Sergeev,[1] Lev V. Soustov,[2] Eugene V. Chelnokov,[2] Nikita M. Bityurin,[2] Peter S. Backlund, Jr,[3] Paul T. Wingfield,[4] Mikhail A. Ostrovsky,[5] and J. Fielding Hejtmancik[1]

Purpose. Exposure to UV-B light (wavelength, 290–320 nm) is a well-documented risk factor for age-related cataracts. As the lens ages, β-crystallins tend to undergo proteolytic cleavage of their terminal extensions. To delineate the effects of loss of terminal arms on β-crystallin function, the sensitivity of purified recombinant wild-type (rβA3) to UV-irradiation induced aggregation was compared with that of βA3-crystallin missing the N-terminal extension (rβA3tr).

Methods. Proteins were expressed in baculovirus-infected Sf9 cells and purified by chromatography. Purified protein solutions (pH 7.4) were reduced by using Tris (2-carboxyethyl) phosphine HCl and irradiated with a 308-nm excimer laser at physiologically relevant UV doses and wavelengths (308 nm), and light-scattering (633 nm) was measured. Irradiated crystallins were analyzed by matrix-assisted desorption ionization (MALDI) and tandem liquid chromatography/mass spectrometry (LC-MS/MS).

Results. UV-irradiation of both rβA3 and rβA3tr resulted in major loss of soluble protein, as shown by absorption at 280 nm, size-exclusion chromatography (SEC) and SDS-PAGE, with concomitant formation of insoluble aggregates producing light-scattering. Compared with wild-type rβA3, rβA3tr showed a significant tendency to begin scattering light at lower UV dose and had a higher aggregation rate with increasing UV exposure. Changes in irradiated crystallins include aggregation and cross-linking, photolysis, and oxidation of methionine and tryptophan residues.

Conclusions. Loss of β-crystallin terminal arms appears to increase their tendency to aggregate in response to UV irradiation, suggesting that this loss in the maturing lens may increase susceptibility to age-related cataract. (*Invest Ophthalmol Vis Sci.* 2005;46:3263–3273) DOI:10.1167/iovs.05-0112

Lens crystallins have a major role in establishing and maintaining lens transparency. Major classes of ubiquitous crystallins include the α-crystallins, which are molecular chaperones related to the small heat shock proteins,[1] and the βγ-crystallins, which are related to bacterial wall and spore-coat proteins.[2–4] The βγ-crystallins share a common two-domain structure.[5–7] Each domain comprises two Greek-key motifs formed by two twisted β-pleated sheets. The β-crystallins also have N- and C-terminal extensions or "arms."[8] As they are studied in solution, β-crystallins associate into higher-order complexes that can undergo rapid subunit exchange, whereas the γ-crystallins exist as stable monomers.[9–13]

Cataracts, a major cause of blindness worldwide, are the clinical result of light-scattering by the lens. This light-scattering can result from loss of cellular order in the lens as a result of disrupted lens development or uncontrolled cell division, or loss of transparency within individual lens cells. The latter can result from aberrations of or damage to the lens crystallins or the intracellular environment, disrupting the ability of the crystallins to interact in a close and orderly fashion and causing them to aggregate or to precipitate. Mutant crystallins can cause hereditary cataracts due to altered stability, association, or solubility. It has been shown recently that splice and deletion mutations of rβA3-crystallin are associated with the formation of autosomal dominant zonular cataract.[14–17] Changes in αA- and αB-,[18–22] βB1-,[23] βB2-,[24,25] γC-, and γD-crystallins[15,26–32] are also associated with congenital cataracts. Thus, it seems possible that structural modifications of lens crystallins may make them more susceptible to further damage by UV-light, resulting in increasing susceptibility to age-related cataract.

As shown by x-ray diffraction analysis, β- and γ-crystallins lose their native structural organization in senile nuclear cataract, and similar changes are observed on UV irradiation of bovine crystallins solutions.[33] Although little is known about the effects of UV exposure on individual βγ-crystallins, the susceptibilities of mixed lens βγ-crystallins to UV radiation have been well characterized,[34–37] supporting earlier results that β-crystallins are more resistant to UV-induced photoaggregation than are γ-crystallins.[34,38] The structures of the β- and γ-crystallin central domains are very similar. However β-crystallins have N- or both N- and C-terminal arms, whereas γ-crystallins have only rudimentary extensions,[39] raising the possibility that differences in β- and γ-crystallin photobehavior may be explained by the presence of terminal arms on β-crystallins.

To investigate this possibility, we applied physiologically relevant doses of UV irradiation to samples of wild-type and N-arm–truncated βA3-crystallins. Structural modifications in βA3tr induced by UV treatment were characterized by MS. Insoluble protein aggregates formed earlier and at a higher rate with the truncated rβA3tr compared to the wild-type protein. The increase in sensitivity of rβA3tr to UV light suggests that the loss of the N-terminal arm from lens β-crystallins may increase their tendency to aggregate under UV-irradiation–induced photo-oxidation, increasing susceptibility to age-related cataract.

From the [1]National Eye Institute, the [3]National Institute of Child Health and Human Development, and the [4]National Institute of Arthritis and Musculoskeletal and Skin Diseases, National Institutes of Health, Bethesda, Maryland; the [2]Institute of Applied Physics, Nizhnii Novgorod, Russia; and the [5]Institute of Biochemical Physics, Moscow, Russia.

Submitted for publication January 28, 2005; revised May 11, 2005; accepted June 30, 2005.

Disclosure: **Y.V. Sergeev**, None; **L.V. Soustov**, None; **E.V. Chelnokov**, None; **N.M. Bityurin**, None; **P.S. Backlund, Jr**, None; **P.T. Wingfield**, None; **M.A. Ostrovsky**, None; **J.F. Hejtmancik**, None

The publication costs of this article were defrayed in part by page charge payment. This article must therefore be marked "*advertisement*" in accordance with 18 U.S.C. §1734 solely to indicate this fact.

Corresponding author: Yuri V. Sergeev, NEI/NIH, 10/10B10, 10 Center Drive, Bethesda, MD, 20892; sergeev@helix.nih.gov.

METHODS

Expression and Purification of rβA3- and rβA3tr-Crystallins

Both rβA3 and rβA3tr were expressed in a baculovirus expression system and prepared as previously described.[10,11,40,41] In rβA3tr, the N-terminal residues 1-29 of βA3-crystallin were removed, and residue 30 was mutated (W30G) to resemble the N-terminal of γB-crystallin. Briefly, Sf9 cells were infected with recombinant AcMNPV virus containing rβA3 or rβA3tr coding sequences. Sf9 cells were harvested in 72 hours, washed with PBS, and stored as a pellet at −70°C. The frozen infected insect cells were lysed by freeze thawing in 1 mL of buffer A: 50 mM Tris HCl (pH 7.5), 1 mM EDTA, 1 mM dithiothreitol (DTT), 150 mM NaCl, 50 μM Tris(2-carboxyethyl)-phosphine (TCEP; Pierce, Rockford, IL), and 2.8 mM thiol protease inhibitor E-64 (Roche Diagnostics, Indianapolis, IN). The lysates were centrifuged at 10,600*g* for 30 minutes at 4°C and were dialyzed against 1 L of buffer A for 24 to 48 hours. Proteins were purified using a fast protein liquid chromatography (FPLC) workstation (Biological Duo-Flow; Bio-Rad, Hercules, CA) at room temperature (20°C). Protein purification was performed as follows. Soluble extracts were loaded onto a 124-mL 16/60 size-exclusion column (Sephacryl S-200 HR; GE Healthcare, Piscataway, NJ) equilibrated with buffer A and eluted at flow rate of 0.5 mL/min. The purity of rβA3 was satisfactory after SEC, and the protein was subjected to UV irradiation after exchanging buffer to fresh buffer A using a Superdex 75 10/30 HR chromatography column (GE Healthcare, Piscataway, NJ). A concentrated sample of rβA3tr was loaded on a 5-mL ion-exchange column (HiTrap DEAE-10; GE Healthcare) and equilibrated with buffer B (50 mM Tris HCl [pH 8.5], 1 mM EDTA, 1 mM DTT, 50 μM TCEP), and 2.5-mL fractions were eluted at a flow rate of 0.5 mL/min and a 500 mL 0 to 1 M NaCl salt gradient was applied.

The location of recombinant proteins among column fractions was determined by monitoring the column eluate at absorbance (A)280 nm and by electrophoresis of aliquots on 12% SDS-PAGE.[42] The identities of rβA3 and rβA3tr were verified by SDS-PAGE and Western blot analysis. The protein concentration of untreated samples was measured by absorption spectroscopy at 280 nm using a spectrophotometer (DU-650 UV; Beckman Instruments, Fullerton, CA).

UV Irradiation of Recombinant β-Crystallins

Before UV-irradiation, protein samples were exchanged by dialysis into buffer C: 1× PBS (pH 7.2), 1 mM DTT, and 50 μM TCEP. UV irradiation of rβA3 and rβA3tr was performed at the Institute of Applied Physics of the Russian Academy of Sciences to which samples were shipped on dry ice (−70°C). Experimental measurements were performed as described earlier.[38] Briefly, 350-μL protein samples (−70°C) were brought quickly to room temperature (20°C) 1 hour before UV-treatment, centrifuged at 5000*g* for 15 minutes at 20°C, and irradiated with an excimer laser LPX-200 (Lambda Physik, Acton, MA) at $\lambda = 308$ nm (XeCl). Temperature variation of protein samples under UV irradiation did not exceed 1°C to 2°C. During sample irradiation, the excimer laser pulse power density was 75 mJ/cm^2 with a pulse repetition rate of 2 pulses/sec. The energy of the excimer laser pulses and protein absorption at 308 nm were measured (ED-200 joulemeter; Gentec, Inc., Quebec City, Quebec, Canada). An HeNe laser (10 mW, $\lambda = 633$ nm) with a beam divergence of 1.1×10^{-3} rads was used as a test beam, to measure light-scattering in a direction perpendicular to the excimer laser beam. The scattered radiation power of a test beam was obtained by the dark-field method with a 633 nm photodiode. Thus, changes in protein absorption at 308 nm and light-scattering at 633 nm were measured in a cuvette simultaneously during the experiment. The energy of UV irradiation (UV dose) was estimated by using the expression $W = 0.15 \times t$ J/cm^2, where t is in seconds. After irradiation, samples were frozen and shipped on dry ice (−70°C) by courier to the National Institutes of Health (Bethesda, MD) for further analysis. The significance of changes in the absorption curves of test samples was estimated by using a fit comparison tool (implemented in Origin 7; OriginLab Corp., Northampton, MA).

All UV-treated protein samples were subjected to centrifugation at 20,800*g* for 30 minutes at 4°C. The pellet of insoluble protein from each sample was resuspended in 4% SDS and analyzed by SDS-PAGE. Supernatant fractions were used for fluorometric analysis, absorption spectra, size-exclusion chromatography (SEC) and SDS-PAGE, and Western blot, as described in the following.

Fluorescence was measured with a spectrofluorometer (Cary Eclipse; Varian Pty. Ltd., Clayton, Victoria, Australia) equipped with 96-well reader. Corresponding to each UV dose, 125-μL rβA3tr samples were diluted in buffer C to a final volume of 250 μL. Tryptophan and *N*-formylkynurenine fluorescent spectra were obtained with 295- and 330-nm excitation wavelengths, respectively. Trp and *N*-formylkynurenine emit fluorescent light at wavelengths of 300 nm and 440 nm, respectively.

Absorption spectra were measured with a spectrophotometer (DU-650 UV; Beckman). Absorption of 10- μL soluble protein samples was scanned from 240 to 320 nm. All UV-irradiated sample absorption values were normalized to those of untreated sample spectra at wavelength of 250 nm. Difference spectra were obtained by measuring absorption of a UV-irradiated sample minus that of an untreated control sample.

Untreated and UV-irradiated soluble fractions of protein samples were analyzed by SEC in buffer C (UV-irradiation of recombinant β-crystallins). Samples (0.1 mL) were loaded on a 10/30 column (Superdex 75 HR; GE Healthcare) and chromatographed at 0.5 mL/min. Void and column volumes were 8.3 and 18.6 mL, respectively. Sample concentrations were 10 μM for the nonirradiated samples. Protein standards used in SEC were bovine serum albumin, ovalbumin, carbonic anhydrase, chymotrypsinogen A, and cytochrome *c*. Chromatographic peaks were integrated by standard methods after baseline subtraction (Origin 7.0; OriginLab, Corp.).

SDS-PAGE, Western blot analysis, and image analysis were performed with 14-μL aliquots (4%) of the supernatant samples. Western blot analysis of antisera raised in rabbits against a synthetic peptide corresponding to residues 36-68 of murine βA3-crystallin was performed separately for supernatant and pellet fractions of rβA3 and rβA3tr. No significant alterations in absorption spectra or SEC and only minimal alterations on Western blot analysis of insoluble proteins were noted in untreated control samples shipped with the test samples. SDS-PAGE gels and Western blot nitrocellulose membranes were digitized and processed with image-analysis software (Scion Image, ver. beta 4.0.2; Scion Corp., Frederick, MD). The cross-section of each gel lane was integrated, and an averaged lane profile was obtained along the protein migration line and saved to disk. Gel and Western blot peaks were integrated after baseline subtraction (Origin, ver. 7.0; OriginLab, Corp.).

Mass Spectrometry Analysis

Samples of rβA3tr (control or UV treated; 4 μg in 0.1 M ammonium bicarbonate) were digested with 0.1 μg trypsin overnight at 37°C. The resultant peptides were reduced with 3 mM 2-mercaptoethanol for 30 minutes at 37°C and alkylated with 10 mM iodoacetamide. The peptides were concentrated by vacuum centrifugation and brought up to 10 μL with 0.1% trifluoroacetic acid (TFA). Contaminating salts and particulates were removed by binding the peptides to a C_{18}-column (ZipTip; Millipore, Bedford, MA), washing with 0.1% TFA, and eluting into 10 μL of an equal volume ratio of 0.1% TFA in water and acetonitrile.

Peptides were analyzed by matrix-assisted desorption ionization (MALDI) mass spectrometry, using a matrix of α-cyano 4-hydroxy cinnamic acid, and by tandem liquid chromatography/mass spectrometry (LC-MS/MS). LC was performed on a commercial system (Magic HPLC; Michrom BioResources, Auburn, CA), with a constant pressure splitter to reduce the flow rate to 400 nL/min. Peptides were separated

with a 75-μm inner diameter fused silica capillary column (PicoFrit; New Objective, Woburn, MA), packed with approximately 5 cm of resin (5 μm particle, 300 angstrom pore; C_{18}; Vydac, Hesperia, CA) followed by separation in buffer A (5% acetonitrile in water with 0.5% acetic acid and 0.005% TFA), using a linear gradient from 2% to 85% of buffer B (80% acetonitrile, 10% *n*-propanol, 10% water), with 0.5% acetic acid and 0.005% TFA. The LC effluent was electrosprayed directly into the sampling orifice of a mass spectrometer (LCQ DECA; Thermo Finnigan, San Jose, CA) using an adaptation of a microscale electrospray interface.[43] The spectrometer was operated to collect MS/MS spectra in a data-dependent manner, with up to three of the most intense ions being subjected to isolation and fragmentation. MS/MS data were analyzed and matched to protein sequences in the database using either the SEQUEST[44] or MASCOT[45] search programs.

Light-Scattering Analysis by the Hill Formula

The concentration of soluble protein in irradiated samples decreased proportionally to the UV dose, as shown in detail in the Results. This suggests that the concentration of denatured protein (D) in solution increases in proportion to the UV dose W (i.e., $[D] \sim W$). By analogy with the Hill formula, the saturation Y can then be calculated as $Y = V_{max}(Wk_a)^b/(1 + (Wk_a)^b$, where, b is a parameter similar to the Hill coefficient, k_a is a value proportional to the microscopic association constant (units: cm^2/JM), W is the UV dose, and $V_{max} = 1$ for the normalized scattering curve. Using a nonlinear fitting algorithm (Origin 7.0, OriginLab Corp.), we fit this equation to the normalized photokinetic data shown by rβA3 and rβA3tr. The resultant plot, by analogy to the Hill plot, shows $\log(Y/1 - Y)$ as a function of $\log(Wk_a)$ with the binding coefficient b, analogous to the Hill coefficient, determined from the expression: $\log(Y/1 - Y) = b \log(Wk_a)$.

Results

Kinetics of UV-Light–Induced Photoaggregation

Protein samples in buffer containing TCEP were treated with 308-nm UV light. The laser light-scattering curves obtained for rβA3 and rβA3tr shown in Figure 1 had a sigmoid shape similar to that described previously.[36,38] As the UV dose increased, there was an increase in light-scattering at 633 nm, reflecting increasing turbidity of the protein solutions (Fig. 1A) and a corresponding decrease in transmittance at 308 nm (Fig. 1B). Both of these correspond to UV-light–induced photoaggregation of protein (i.e., the transition from soluble to insoluble protein, as described later). Both the transmission and scattering curves shown in Figure 1 show that the N-arm deleted mutant rβA3tr is more susceptible to UV-induced aggregation than the wild-type protein (rβA3), although this is shown more dramatically by the light-scattering data.

Quantitative photokinetic parameters (the energy threshold W_t and aggregation rate V) estimated from the data shown in Figure 1 are given in Table 1. The ratios of aggregation rates (V_m/V_{wt}) derived from the transmittance curves at 308 nm show only a small difference for rβA3 and rβA3tr (0.0083 ± 0.0004 and 0.0090 ± 0.0004 J/cm^2 respectively), giving a ratio V_m/V_{wt} of 1.08 (Table 1). However, the ratios of aggregation rates (V_m/V_{wt}) derived from the light-scattering data at 633 nm show more significant differences of 0.0074 ± 0.0001 (rβA3) and 0.0117 ± 0.0002 (rβA3tr) J/cm^2, giving a ratio of 1.58. Both transmittance and light-scattering data demonstrate a higher sensitivity (lower threshold) for rβA3tr than for rβA3. The threshold energies (W_t) for βA3 versus βA3tr are 71 ± 1 versus 39 ± 2 and 26 ± 3 versus 9 ± 4 for the transmittance curves at 308 nm and the light-scattering data at 633 nm respectively, both showing an lower sensitivity threshold for rβA3tr compared with rβA3.

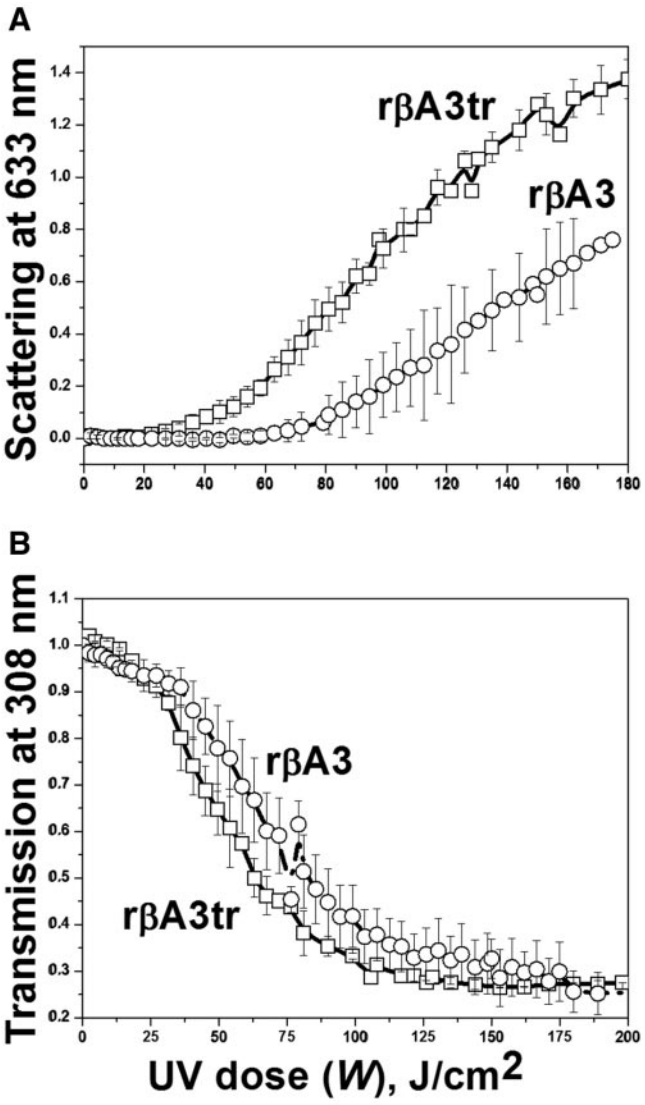

Figure 1. Changes in transmission (308 nm) and light-scattering (633 nm) obtained on UV irradiation of 10-μM samples of rβA3 and rβA3tr. Light-scattering data at 633 nm (**A**) and UV-light transmission at 308 nm (**B**) are shown as a function of UV dose. Shown are experimental points and results of curve fitting to the experimental data for rβA3 and rβA3tr. Standard errors demonstrating the reproducibility of measurements between different samples of the same protein are shown for each curve.

Absorption curves from light-scattering shown in Figure 1A or derived from the transmission shown in Fig. 1B were compared by fitting the same regression curve (see the Hill function in the Methods section) using a fit comparison tool implemented (Origin, ver. 7.0; OriginLab Corps.). Although fitting of the 308-nm absorption data shows no significant difference between rβA3 and rβA3tr data sets ($F = 0.91$; $P = 0.46$), differences in the curves of rβA3 and rβA3tr at 633 nm were statistically significant ($F = 19.99$; $P = 1.19E\text{-}9$). However, overall both the aggregation rate and lower threshold energy demonstrate that truncated rβA3tr is more sensitive to UV irradiation than is wild-type rβA3.

SEC of UV-Light–Treated rβA3 and rβA3tr

Samples of rβA3 and rβA3tr irradiated with UV-light doses from 25 to 175 J/cm^2 with 25 J/cm^2 increments were analyzed by

TABLE 1. Photokinetic Parameters Estimated from Light-Scattering (633 nm) and Transmission (308 nm) Data

λ (nm)	Protein	W_t (J/cm^2)	V (cm^2/J)	Ratio
308	βA3tr	9 ± 4	0.0090 ± 0.0004	1.08 ± 0.0008
	βA3	26 ± 3	0.0083 ± 0.0004	
633	βA3tr	39 ± 2	0.0117 ± 0.0002	1.58 ± 0.0003
	βA3	71 ± 1	0.0074 ± 0.0001	

Parameters at wavelength 308 nm estimated from absorption data (not shown), which were derived from transmission curves (Fig. 1B). The threshold energy (W_t), corresponding to the beginning of protein photoaggregation and obtained by extending the ascending linear part of the kinetic curve back to the W intercept, estimates the minimum energy of the UV light necessary to initiate detectable light-scattering (Fig. 1A). The second parameter, the aggregation rate (V), corresponding to the tendency of soluble protein to aggregate is obtained as the slope of the ascending linear part of the curve and shows the rate of change of the relative intensity of scattering per energy interval at energies above the threshold. The ratio is calculated as V_m/V_{wt}, where V_m and V_{wt} are the aggregation rates for the mutant (rβA3tr) and wild-type (rβA3) proteins, respectively. The parameters W_t, V, and errors (shown in parenthesis) were estimated by using a linear fit in the central part of corresponding scattering curve.

protein absorption spectroscopy, SEC, SDS-PAGE, and Western blot analysis. The SEC and absorption data were obtained for the soluble fraction of rβA3 and rβA3tr after removing insoluble protein by centrifugation. Aliquots of soluble fractions of rβA3 and rβA3tr irradiated with doses from 25 to 100 J/cm^2 were chromatographed (Superdex 75 column; GE Healthcare; Fig. 2). Nonirradiated rβA3 and rβA3tr samples show single major peaks eluting at 11.1 and 12.9 mL, respectively, corresponding to apparent molecular weights of 29.5 and 23.0 kDa similar to those published earlier.[10]

Irradiated samples of both rβA3 and rβA3tr show a decrease in the height of the major peak proportional to the level of irradiation (Fig. 2). However, the peak heights of the rβA3tr samples decrease more markedly than those of rβA3, consistent with the transmission data. There is little or no shift of elution position with increasing UV irradiation, although the peaks broaden somewhat, especially on their trailing ends. The rβA3tr samples irradiated with 25 J/cm^2 show a new peak at 11 mL. This peak is minimally present in the control sample and decreases markedly with increasing levels of irradiation. It is not present in the rβA3 samples to any appreciable extent.

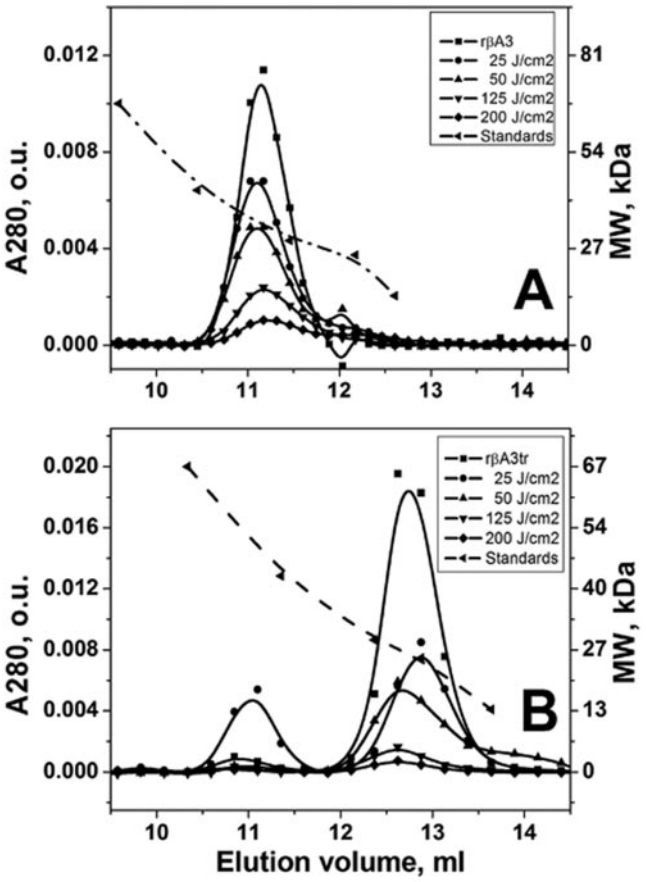

FIGURE 2. Chromatographic profiles of the soluble fractions of rβA3 (**A**) and rβA3tr (**B**) obtained after UV-light irradiation. Untreated and UV-light irradiated samples are shown, as indicated.

Western Blots of UV-Light–Treated rβA3 and rβA3tr

Western blot analysis of the UV-treated rβA3 and rβA3tr samples are shown in Figure 3. The soluble protein samples showed progressive loss of staining intensity for the major bands at 27 kDa (rβA3) and 23 kDa (rβA3tr) as the UV dose increased from 25 to 200 J/cm^2. This loss was greater for rβA3tr than for rβA3 at higher UV doses (Figs. 3A, 3C) and was accompanied in the 25-, 50-, and 75-J/cm^2 samples by the appearance of additional bands of 23 and 18 kDa (rβA3), and 18 kDa (rβA3tr), along with increased dispersed staining below the major bands for each UV dose. Above the major band, there was an additional band at 52 kDa (rβA3) and 46 kDa (rβA3tr), visible only on the Western blot in the 25- to 125-J/cm^2 (rβA3) and in the 25- to 75-J/cm^2 (rβA3tr) samples, consistent with the appearance of dimers on SEC (Fig. 2).

Western blot analyses of proteins from the insoluble pellets of rβA3 and rβA3tr showed the major 27-kDa rβA3 (Fig. 3B) and 23-kDa rβA3tr (Fig. 3D) bands, respectively. Insoluble rβA3 decreased at energies of UV irradiation higher than 50 J/cm^2, whereas an additional band at 18 kDa decreased slightly at UV doses higher than 100 J/cm^2. The 23-kDa insoluble rβA3tr band decreased at UV doses $W > 75$ J/cm^2, whereas a second 18-kDa band continued to increase until 200 J/cm^2. Smaller immunoreactive peptides were also present diffusely below the major 27-kDa rβA3 and 23-kDa rβA3tr bands. Those samples irradiated with doses between 25 and 175 J/cm^2 showed additional higher-molecular-weight bands at 50 kDa (rβA3) and 46 kDa (rβA3tr), with a faint band also visible in the untreated but transported rβA3 sample (Fig. 3B). These bands were faint in the rβA3tr samples and decreased with increasing UV dose >100 J/cm^2 in the rβA3 samples. In addition, there was a diffuse smear of immunoreactive peptides in the rβA3tr insoluble samples, extending from 17 kDa to more than 100 kDa. SDS-PAGE of the insoluble samples produced faint bands because of the small amounts of protein present in the pellets (data not shown).

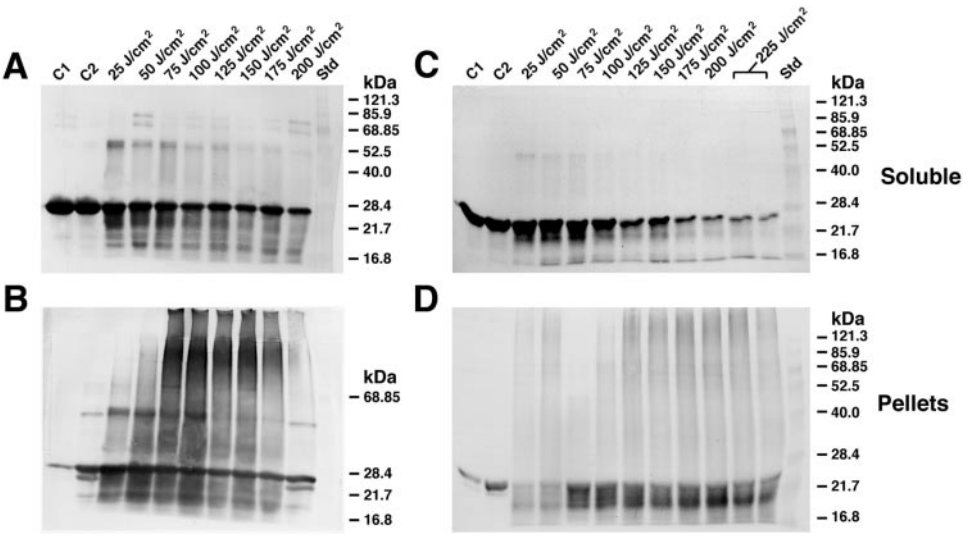

FIGURE 3. Western blot analysis of soluble (**A**, **C**) and insoluble (**B**, **D**) UV-treated rβA3 (**A**, **B**) and rβA3tr (**C**, **D**). *Lanes C1*, *C2*: nonirradiated control samples, with the sample in *lane C1* simply stored frozen and that in *lane C2* having been shipped with the treated samples to control for possible sample degradation during transportation. Other lanes are treated samples irradiated at 308 nm with doses ranging from 25 to 225 J/cm^2 at 25-J/cm^2 increments. *Lane Std*: protein standards.

Characterization of rβA3tr by MS

UV-light-treated rβA3tr samples were digested with trypsin, and the reduced and alkylated peptides were analyzed by MALDI-MS spectrometry to detect the covalent modifications of β-crystallin resulting from exposure to UV light. Major peaks in the MALDI spectra of control samples correspond to amino acid residues 30-44 (m/z 1796.00), 44-63 (m/z 2231.97), 64-89 (m/z 3001.43), 90-108 (2294.03), 95-121 (3176.00), 109-124 (m/z 1904.60), 125-136 (m/z 1466.79), 137-176 (m/z 4736.05), and 177-210 (m/z 4026.83). Thus, the MALDI spectra contained peaks corresponding to tryptic peptides matching approximately 80% of the predicted amino acid sequence. Covalent modifications to rβA3tr due to UV irradiation were detected in MALDI MS by the appearance of additional peaks or by shifts in the mass of a peak in the spectra.

When rβA3tr was exposed to UV irradiation, the peak heights for many of the tryptic peptides were greatly reduced in the MALDI spectra, whereas the peak heights for only a few peptides remained fairly constant, as described in the legend to Figure 4. In addition, several new peaks appeared in the lower m/z range of the spectra, with increasing levels of UV exposure (Figs. 4A, 4B). The changes in the spectra suggest that certain regions of rβA3tr are particularly sensitive to fragmentation by these levels of UV irradiation. After exposure to higher doses of UV irradiation, the amount of intact protein decreased, as seen by the loss of intensity of several MALDI peaks for tryptic peptides from the protein, consistent with the decrease in protein migrating with the intact band on SDS/PAGE (Figs. 3C, 3D). Some of these peaks were not detectable at higher doses (data not shown).

The mass difference between some of these newly formed MALDI peaks, suggests that a ladder of C-terminal fragments is being generated on exposure to UV irradiation (Fig. 4B). To examine the identity of these peaks, samples were analyzed by LC/MS/MS (Table 2). Trypsin cleaves the C-terminal region of rβA3tr to generate a peptide with a predicted mass of 2147.04 (residues 193-210, HWPEWGSHAQTSQIQSIR). This peptide is observed in MALDI spectra and in LS/MS/MS spectra for tryptic digests of the control protein. With increasing UV exposure, the peak in the MALDI spectra of the intact tryptic peptide 193-210 decreased, and a series of peaks consistent with a ladder of peptides ending with R210 were observed (Fig. 4B). Two of the C-terminal fragments (SQIQSIR and QTSQIQSIR) appeared to be present in the control samples, indicating that some breakdown of the rβA3tr occurred during purification or storage (Fig. 4A). The identities were confirmed by LC/MS/MS analysis for five of these peptides (Table 2). Thus, UV exposure under these conditions resulted in extensive fragmentation of rβA3tr at the peptide bonds within the C-terminal region of the protein at positions 193-210.

In addition to fragmenting the protein, exposure to UV irradiation can also result in photo-oxidation.[46] Tryptic peptides from rβA3 were examined for changes in oxidation of methionine and tryptophan residues after exposure to UV irradiation. Oxidation of methionine and tryptophan residues was determined from the ratio of the monoisotopic peak intensities for oxidized and unmodified tryptic peptides in the MALDI spectra (Figs. 4C, 4D). Oxidation of methionine to methionine sulfoxide resulted in an increase of 16 mass units, and tryptophan residues were oxidizable with an increase of 16 mass units by the addition of one oxygen atom or with an increase of 32 mass units by the addition of two oxygen atoms, to form *N*-formylkynurenine.

The four methionine residues in βA3-crystallin are located in three tryptic peptides. Tryptic peptides containing M45 and M110 were observed in the MALDI spectra, along with their corresponding oxidized peptides. A third tryptic peptide, residues 137-161, includes W152, M150, and M160. The MALDI spectra of control samples do not contain a peak at the mass corresponding to this peptide, and so changes to this region of the protein resulting from UV exposure could not be determined. Some oxidation was observed in tryptic digests of the control protein for peptides containing M45 and M110, and the amount of oxidation of both increased significantly with UV exposure (Fig. 4C), more than doubling at doses of 50 J/cm^2 and further increasing dramatically at doses above 150 J/cm^2. This indicates oxidation of methionine with subsequent formation of methionine sulfoxide on exposure to UV.

The eight tryptophan residues are located in five tryptic peptides within the rβA3tr sequence. In the MALDI spectra, peaks corresponding to four peptides with six of the tryptophan residues are observed. For two peptides (residues 95-109 and 193-210), two tryptophan residues were present in each peptide. Tryptic peptide 193-210 was the C-terminal tryptic peptide that exhibited extensive fragmentation with UV exposure (Fig. 4B, Table 2). Two peaks corresponding to oxidation of tryptic peptide 95-109 were observed in the MALDI spectra at m/z 1707.7 and 1723.7, representing the change in mass for the addition of one and two oxygen atoms, respectively (data not shown). Because MS/MS data were not obtained for these

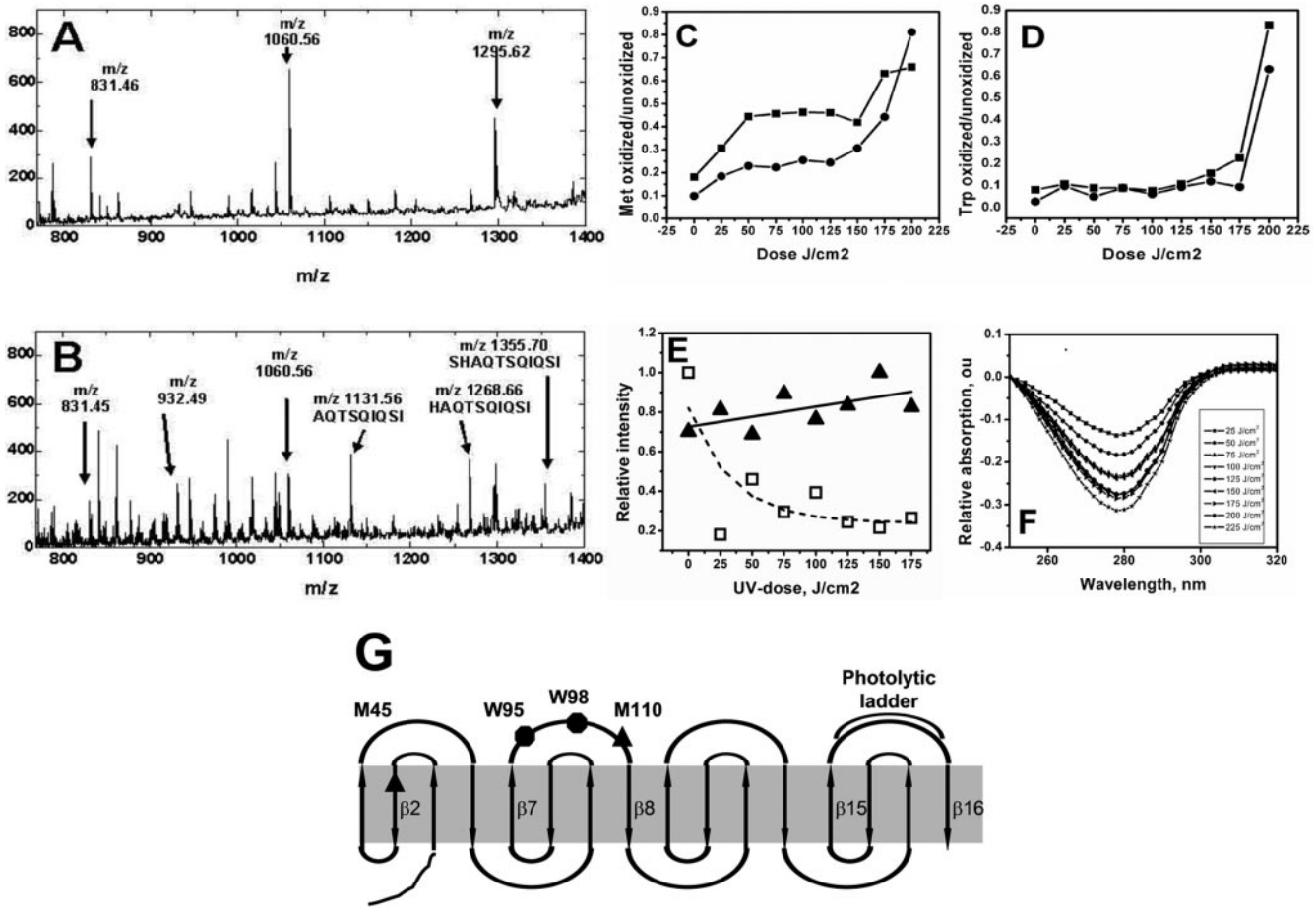

FIGURE 4. MALDI-MS data for tryptic digests and spectral data of UV-light–treated rβA3tr. (**A**, **B**) MALDI spectra in the m/z region from 800 to 1400 for the control and the UV-treated samples at 175 J/cm^2 rβA3tr. Peaks corresponding to predicted masses for fragments of the C-terminal tryptic peptide 193-210 (HWPEWGSHAQTSQIQSIR) are indicated. Methionine and tryptophan oxidation was determined from the ratio of monoisotopic peak heights for reduced and oxidized tryptic peptides. (**C**) Oxidation of tryptic peptides RMEFTSSCPNVSER (residues 44-57, m/z 1699.78; ■) and LMSFRPICSANHK (residues 110-121, m/z 1560.78; ●). (**D**) Oxidation of the tryptophan containing peptide WDAWSGSNAYHIER (residues 95-109, m/z 1691.76) for the mono-oxidized (m/z 1707.76; ●) and dioxidized (m/z 1723.76 ■) peptides. Peaks fairly constant in size at different UV doses were located outside the region included in this figure and included: residues 1-14 (GKITIYDQENFQGK, m/z 1640.83), 1-15 (GKITYDQENFQGKR, m/z 1796.92), 3-15 (ITYDQENFQGKR, m/z 1611.81), 29-34 (NFDNVR, m/z 764.37), and 102-107 (ENFIGR, m/z 735.38). (**E**) Relative fluorescence intensity changes for tryptophan (at 330 nm, □) and *N*-formylkynurenine (at 430 nm, ▲) with UV dose. Fluorescence intensities of tryptophan and *N*-formylkynurenine were normalized by the fluorescence intensities at the UV doses of 25 and 150 J/cm^2, respectively. Experimental points and the related curve (**E**) corresponding to *N*-formylkynurenine were shifted up by +0.5 optical units. (**F**) Absorption of UV-irradiated rβA3tr at 280 nm. Vertical and horizontal axes correspond to relative absorption changes (in optical units) and wavelengths from 240 to 340 nm, respectively. Protein absorption curves at each UV dose were normalized by dividing each value by the A250 of that sample. Relative absorption was calculated as a difference between the normalized absorption of irradiated and untreated protein samples in buffer C at the UV doses as shown. (**G**) The rβA3 Greek-key motif structure with the locations of photolytic modifications identified by MS marked. (▲) Tryptophan and (●) methionine residues modified by UV-light treatment.

oxidized peptides, it is not clear whether the two oxygen atoms were present on a single tryptophan residue, or they were on separate residues. Oxidation of peptide 95-109 with UV exposure was quantitated by the ratio of peak heights for the oxidized and unmodified peptide (Fig. 4D). As opposed to methionines, at low doses of UV light, little increase in tryptophan oxidation was observed, but at higher doses (>150 J/cm^2) tryptophan oxidation increased dramatically.

In addition to the changes found in these specific tryptophan residues by mass spectrometry, total changes in tryptophan content under UV irradiation was quantified using fluorometry and absorption spectrophotometry. Tryptophan residues fluoresced at 330 nm. Under UV-treatment Trp oxidized to *N*-formylkynurenine, which had a maximum fluorescence at 440 nm. Figure 4E shows the change in relative intensities of tryptophan and *N*-formylkynurenine fluorescence in rβA3tr-crystallin with increasing doses of UV irradiation. On average, the intensity of tryptophan fluorescence decreased with increasing UV-B exposure, whereas that of *N*-formylkynurenine increased. These results agree with the absorption data. A significant part of β-crystallin's total absorption at A280 was due to absorption by tryptophan. Figure 4F shows decreasing absorption at 280 nm with increasing UV-B doses, consistent with decreasing tryptophan content due to UV damage.

DISCUSSION

When UV irradiation was applied to samples of rβA3- and truncated rβA3tr-crystallins, formation of insoluble protein developed earlier and at a higher rate for the truncated rβA3tr

TABLE 2. Identification of C-Terminal Fragments from MS/MS Spectra

Peptide Sequence	Predicted MH^+	LCQ MS/MS Observed $[MH_2]^{2+}$	MS/MS MASCOT Ion Score
HAQTSQIQSIR	1268.66	635.0	58
AQTSQIQSIR	1131.56	566.4	50
QTSQIQSIR	1060.54	530.9	44
TSQIQSIR	932.50	466.9	39
SQIQSIR	831.46	416.4	40

Predicted sequences for tryptic peptides resulting from UV-induced fragmentation in the C-terminal region of the protein are indicated in the first column. The predicted protonated masses for these peptides are in the second column, and the observed mass-to-charge of the doubly charged ions used for MS/MS analysis are shown in the third. Peptide sequences were determined by using MASCOT[45] to search the mammalian database. Since peptides resulting from UV-generated cleavage have a trypsin cleavage site at only one end of the peptide, semi-trypsin enzyme specificity was used in the search. The sequences shown were the best fit of the MS/MS spectra to sequences in the database. MASCOT ion score is $-10 \cdot \log(P)$, where P is the probability that the observed match is a random event. Ion scores >44 indicate identity or extensive homology to the matching peptide ($P < 0.05$).

compared with the wild-type protein, accompanied by photolysis and oxidation of methionine and tryptophan residues. This increased sensitivity of truncated rβA3tr to UV-light–induced aggregation suggests that loss of terminal arms may be related to age-related cataractogenesis, for which UV light exposure is known to be a risk factor. βA3-crystallin was chosen for these studies because of the extensive information available about its stability and association properties.[11] Mutations in this crystallin are known to cause cataracts with a variable nuclear morphology and in some cases with sutural and cortical features.[14–17,47] These congenital cataracts are, of course, influenced by developmental regulation of the βA3-crystallin gene in ways that age-related cataracts are not. Although the truncated crystallin used in these studies is not found in nature, it was chosen to provide the best direct estimation of the effect of the amino terminal arm on UV sensitivity. Truncation of the amino terminal arm at a residue normally internal within the terminal arm can inadvertently change the aggregation behavior of β-crystallins, occasionally with dramatic results.[48]

Analysis of UV-treated βA3-crystallins is consistent with the occurrence of several simultaneous molecular processes, also observed in earlier studies.[5,34,38,49] One of these is photooxidation, an oxidative action of free radicals induced in the surrounding solution.[50] This often results in protein cross-linking, initially to form dimers and later to form insoluble aggregates stabilized by intermolecular covalent bonds. In addition, oxidation of amino acids can decrease the solubility of crystallins and contribute to irreversible aggregation. The increasing light-scattering at 633 nm of both rβA3 and rβA3tr solutions irradiated with increasing doses of UV-light (Fig. 1A) results from the formation of insoluble aggregates. These insoluble aggregates are easily removed from the protein solution by low-speed centrifugation and are at least partially solubilized by the presence of reducing agents in the gel sample buffer, suggesting that some cross-linking occurs by formation of disulfide bonds, a major mechanism of cross-linking of photooxidized crystallins.[51] In this light, βA3-crystallin contains eight cysteine residues, almost half of which appear to be sterically available to form intermolecular disulfide bonds, which also explains differences in cross-linking evident on SEC, which would include disulfide bonds, and PAGE, in which samples were highly reduced. In addition, the cross-linking of rβA3tr detected by SEC may represent higher-order aggregates, since this molecule is retained somewhat on SEC columns.[10] Evidence for protein cross-linking was also detected in earlier studies of photo-oxidation of lens derived α-, β-, and γ-crystallins and recombinant βA3-crystallin.[38]

In the current study, the formation of intermolecular disulfide bonds due to UV-light treatment was minimized at low levels of UV exposure, because sample transportation and biochemical analysis were performed in buffer containing 1 mM DTT and 50 μM TCEP. In addition, the SDS-PAGE sample buffer had 2-β-mercaptoethanol reducing disulfide cross-link. The absence of a reducing environment in studies of lens proteins in vitro has been shown to result in differing oxidative changes from the intact lens.[52] Reducing agents were included in the reaction buffer to replicate as closely as possible the intracellular environment of the lens, which has strong reducing capabilities.

A second process in UV-treated crystallins is photolysis, breakage of the amino acid backbone by the direct effect of UV light, acting on tryptophan or other residues. Although both processes could be seen in the soluble and insoluble fractions, even at 25 J/cm^2, *photolysis* tended to predominate at higher UV doses (Fig. 3). Photolysis of sensitive residues in the protein produced the discrete bands representing truncated crystallins and peptides seen on SDS-PAGE at higher UV doses, whereas nonspecific chain scission produced the background smears seen in these lanes.

As summarized in Figure 5, results of peak area change detected by SEC at 280 nm, SDS-PAGE, and Western blot analysis, as well as protein absorption changes at 280 nm, all demonstrated a decrease in soluble protein with increasing UV dose, also consistent with the MS data. This decrease occurred as result of insoluble aggregate formation, which then caused light-scattering. Decreasing light absorption at 308 nm probably is also contributed to by a second process, photomodification of tryptophan residues absorbing UV light at 280 to 290 nm in the remaining soluble protein, as shown by the MS data. This process would be expected to occur in rβA3 and rβA3tr at a similar rate, providing a partial explanation for the smaller differences in their susceptibility to UV irradiation when assessed by transmission than in light-scattering, which would be totally dependent on aggregation. Modification of tryptophan residues in lens proteins in vivo and in vitro due to UV-light irradiation is a well-studied process.[35,53]

These two main types of UV-induced changes were also observed in the protein structure itself by examination of the MALDI spectra. First, there were dramatic losses in the intensity of specific peptides, along with generation of low-mass peaks that appeared to be due largely to fragmentation of the protein at peptide bonds. This observation is consistent with the results of the SEC and Western blot analyses described in the Results section. The second type of change observed was

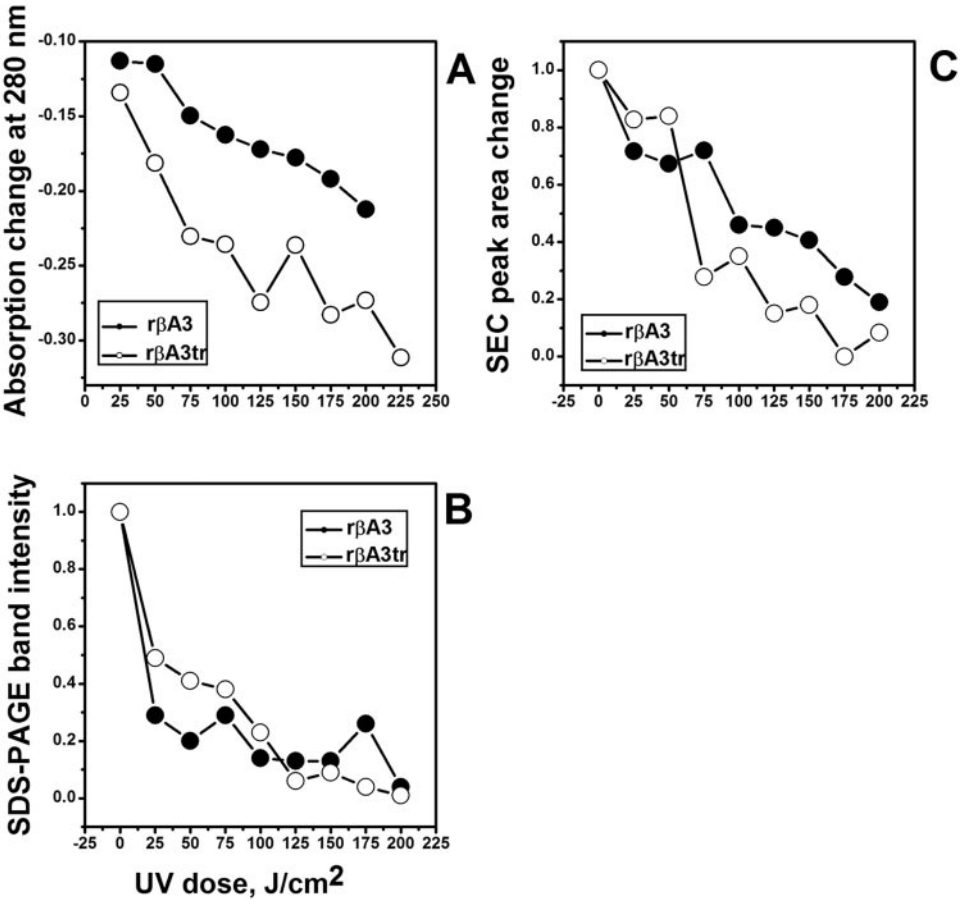

FIGURE 5. Absorption decrease obtained by spectral measurements, SEC and SDS-PAGE band intensity change after UV treatment. (**A**) Absorption change at 280 nm derived from Figure 2. (**B**) Relative change in SDS-PAGE band intensity for soluble fractions, obtained as described in the Methods section and normalized to the control sample band intensity. (**C**) Relative change in chromatographic peak area relative change, normalized to the area of nonirradiated sample and calculated independently for each protein (rβA3 and rβA3tr).

oxidation of peptides containing methionine and tryptophan. Although SEC and SDS-PAGE data suggest possible protein cross-linking (Fig. 3), evidence for specific cross-linking between peptides currently was not observed in MS data, perhaps because of several factors, one of which is that the cross-linked peptides would have a large mass that would make it difficult to detect under the types of MS used in this study.

From the loss of peak intensity for specific peptides, it appears that specific regions of rβA3tr show increased susceptibility to fragmentation by UV treatment. Although the specific mechanism for peptide fragmentation by UV treatment is not clear from these experiments, regions of the protein containing tryptophan residues appear to be particularly prone to fragmentation by UV treatment. One of these is the C-terminal peptide 199-203 (which has two tryptophan residues nearby: W194 and W197), located in the loop connecting strands β15 and β16 in the fourth Greek-key motif of βA3-crystallin (Fig. 4G). The observed accessibility to photolysis of residues in positions 200-204 (Table 2) is consistent with the prediction that this loop is exposed at the protein surface, which may make it more susceptible to the UV treatment.[10]

The oxidation of methionine residues to methionine sulfoxide increases the surface hydrophobicity of protein[54] and may decrease its solubility. The MS data showed an increase in methionine oxidation under UV-treatment (Fig. 4C). This suggests that in certain conditions oxidized methionines may promote the formation of higher-molecular-weight aggregates. Identification of methionine oxidation as a major result of UV irradiation of β-crystallins is particularly notable, in that reduction of methionine sulfoxide by methionine sulfoxide reductase A has recently been shown to be critical for cultured lens cell survival under both normal culture conditions and oxidative stress.[55] Modification of tryptophan residues in lens proteins in vivo and in vitro due to UV irradiation is well described.[35,53] In the present study oxidation of two tryptophans in positions 95 and 98 (Fig. 4D) was observed, and the relative oxidation of those tryptophan residues increased with treatment at higher UV doses. In addition, decreases in the total tryptophans content with UV treatment were shown by tryptophan fluorescence and absorption measurements. At present, we are using MS to understand further the role of methionine, tryptophan, and other residues in higher-molecular-weight aggregate formation and to identify specific structural modifications of the protein that are associated with UV-light treatment.

Comparison of the effect of UV irradiation on rβA3 and rβA3tr provides insight into the effects of the well-documented loss of β-crystallin terminal extensions in developing and aging lens fibers and in some forms of cataracts[56] on the sensitivity of the lens to UV light.[57–59] Because both proteins share identical amino acid sequences for most of their structure, differing only by absence of the N-terminal 29 amino acid terminal arm in rβA3tr ($<$15%), similar photokinetics in response to UV light may be expected. The truncated rβA3tr protein is "capped" with a glycine residue similar to that in γB-crystallin, which might be expected to prevent untoward reactions of amino acids inadvertently exposed to solvent.[48] However, rβA3tr-crystallin appears to be more susceptible to UV-light treatment than the rβA3-crystallins and possibly even to oxidative damage from routine handling and shipping. This suggests a protective role against UV light and oxidative damage for the βA3-crystallin N-terminal extension.

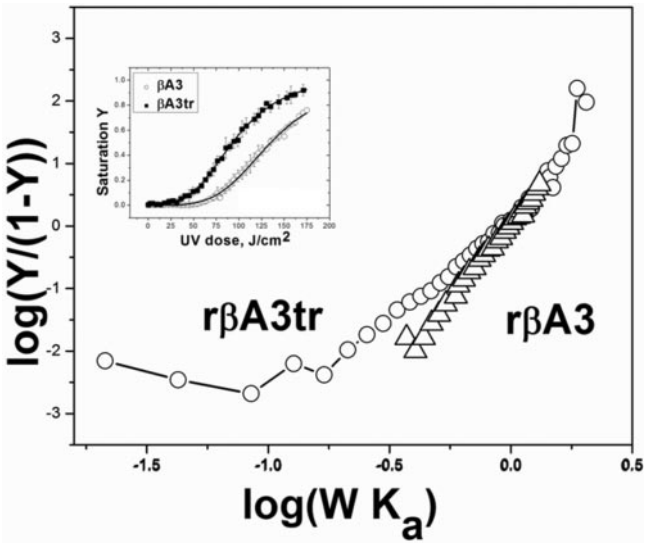

FIGURE 6. Plot similar to Hill plot showing $\log(Y/1 - Y)$ as a function of $\log(Wk_a)$, as estimated from 633-nm light-scattering data for rβA3 and rβA3tr (Fig. 1A). The saturation Y as function of UV dose is shown in *inset*. This parameter was calculated from data presented on Fig. 1A.

Although the analogy is inexact, one way to conceptualize aggregation of β-crystallins is as a bimolecular association. In a fashion analogous to the Hill plot, the saturation curve Y can be fitted to the data as shown in the inset in Figure 6. W_o (22–27 J/cm^2), as estimated from the Hill plot (Fig. 6), is the UV dose necessary to achieve recognizable aggregation of protein induced by UV light. For $W > W_o$ the binding coefficients b are greater than 1 for both rβA3 and rβA3tr (4.15 ± 0.16 and 3.34 ± 0.11, respectively). By analogy with the Hill coefficient, values of the binding coefficient b greater than 1 suggest that scattering, which results from aggregation of denatured protein with increasing UV dose, is a positively cooperative process for both rβA3 and rβA3tr. This more than linear response of aggregation to UV irradiation indicates that the presence of denatured protein increases the UV susceptibility of crystallins still in solution. At UV doses $W < W_o$ the binding coefficient is <1 (rβA3tr), which may indicate a protective effect of the antioxidants in the buffer at low UV doses, the intrinsic resistance of the protein itself to photo-oxidation or perhaps that UV damage initially is accumulated in soluble protein.

In an earlier epidemiologic study, an association was identified between UV-B (wavelengths from 290 to 320 nm) exposure and age-related cataract in the human lens.[60] From the amount of solar UV-B reaching the Earth's surface (approximately 2×10^{-4} W/cm^2), the human lens receives ($0.0012–0.01$) $\times 10^{-4}$ W/cm^2 of UV-B radiation in vivo.[61] The yearly accumulation of UV-light exposure received by the human lens may be estimated from these data, assuming 240 sunny days a year, to be 2.5 to 20.6 J/cm^2, giving an average yearly accumulation of lens exposure of 11.5 J/cm^2. The maximum UV dose of 200 J/cm^2 applied to rβA3 and rβA3tr solutions in our experiments at a wavelength of 308 nm within the UV-B range was equivalent to the cumulative UV radiation received by the human lens within approximately 20 years. Although the lens has metabolic systems that maintain a reducing environment,[62] these decline with age and in cataractous lenses.[63] Thus, although in these experiments UV irradiation was delivered at a high rate over a short period, the results represent physiologically relevant UV radiation levels and allow in vitro modeling of the effect of UV-B damage to individual crystallins and their modified forms during lens aging and cataract development in humans.

In summary, physiologically relevant doses of UV irradiation were applied to samples of wild-type and mutant βA3-crystallins reduced with the disulfide bond breaker TCEP. The shapes of photokinetic curves of rβA3- and rβA3tr-crystallins both show an initial lag followed by increasing aggregation with increasing UV irradiation. However, light-scattering related to formation of insoluble protein aggregates develops earlier for rβA3tr, which also has a higher aggregation rate than that of rβA3. Molecular changes identified in rβA3tr include both photolysis and oxidation of methionine and tryptophan residues. The difference in sensitivity to UV light of normal and truncated recombinant βA3-crystallins suggests that loss of terminal extension during lens maturation and aging increases the tendency of β-crystallin to aggregate under UV irradiation, increasing susceptibility to age-related cataract.

Acknowledgments

Authors thank Alfred Yergey (Laboratory of Cellular and Molecular Biophysics, Section on Metabolic Analysis and Mass Spectrometry, National Institute of Child Health and Human Development, National Institutes of Health) for stimulating discussions on mass spectroscopy data and Rafael Caruso (Ophthalmic Genetics and Visual Function Branch, National Eye Institute), who brought to our attention papers on earlier epidemiologic studies of the association between UV-B radiation and age-related cataract.

References

1. Horwitz J. Alpha-crystallin can function as a molecular chaperone. *Proc Natl Acad Sci USA*. 1992;89:10449–10453.
2. Wistow G, Summers L, Blundell T. Myxococcus xanthus spore coat protein S may have a similar structure to vertebrate lens beta gamma-crystallins. *Nature*. 1985;315:771–773.
3. Bagby S, Harvey TS, Eagle SG, Inouye S, Ikura M. NMR-derived three-dimensional solution structure of protein S complexed with calcium. *Structure*. 1994;2:107–122.
4. Clout NJ, Kretschmar M, Jaenicke R, Slingsby C. Crystal structure of the calcium-loaded spherulin 3a dimer sheds light on the evolution of the eye lens betagamma-crystallin domain fold. *Structure* (*Camb*). 2001;9:115–124.
5. Wistow G, Turnell B, Summers L, et al. X-ray analysis of the eye lens protein gamma-II crystallin at 1.9 A resolution. *J Mol Biol*. 1983;170:175–202.
6. Sergeev YV, Chirgadze YN, Mylvaganam SE, et al. Surface interactions of gamma-crystallins in the crystal medium in relation to their association in the eye lens. *Proteins*. 1988;4:137–147.
7. White HE, Driessen HPC, Slingsby C, Moss DS, Lindley PF. Packing interactions in the eye-lens: structural analysis, internal symmetry and lattice interactions of bovine gamma IVa-crystallin. *J Mol Biol*. 1989;207:217–235.
8. van Rens GLM, Raats JMH, Driessen HPC, et al. Structure of the bovine eye lens gammaS-crystallin gene (formerly betaS). *Gene*. 1989;78:225–233.
9. Hejtmancik JF, Wingfield P, Chambers C, et al. Association properties of beta-B2- and betaA3-crystallin: ability to form dimers. *Protein Eng*. 1997;10:1347–1352.
10. Sergeev YV, Wingfield PT, Hejtmancik JF. Monomer-dimer equilibrium of normal and modified beta A3-crystallins: experimental determination and molecular modeling. *Biochemistry*. 2000;39:15799–15806.
11. Sergeev YV, Hejtmancik JF, Wingfield PT. Energetics of domain-domain interactions and entropy driven association of beta-crystallins. *Biochemistry*. 2004;43:415–424.
12. Bax B, Lapatto R, Nalini V, et al. X-ray analysis of beta B2-crystallin and evolution of oligomeric lens proteins. *Nature*. 1990;347:776–780.

13. Lapatto R, Nalini V, Bax B, et al. High resolution structure of an oligomeric eye lens beta-crystallin: loops, arches, linkers and interfaces in betaB2 dimer compared to a monomeric gamma-crystallin. *J Mol Biol*. 1991;222:1067–1083.
14. Kannabiran C, Rogan PK, Olmos L, et al. Autosomal dominant zonular cataract with sutural opacities is associated with a splice site mutation in the βA3/A1-crystallin gene. *Mol Vision*. 1998;4:21.
15. Burdon KP, Wirth MG, Mackey DA, et al. Investigation of crystallin genes in familial cataract, and report of two disease associated mutations. *Br J Ophthalmol*. 2004;88:79–83.
16. Qi Y, Jia H, Huang S, et al. A deletion mutation in the betaA1/A3 crystallin gene (CRYBA1/A3) is associated with autosomal dominant congenital nuclear cataract in a Chinese family. *Hum Genet*. 2004;114:192–197.
17. Bateman JB, Geyer DD, Flodman P, et al. A new betaA1-crystallin splice junction mutation in autosomal dominant cataract. *Invest Ophthalmol Vis Sci*. 2000;41:3278–3285.
18. Litt M, Kramer P, LaMorticella DM, et al. Autosomal dominant congenital cataract associated with a missense mutation in the human alpha crystallin gene CRYAA. *Hum Mol Genet*. 1998;7:471–474.
19. Berry V, Francis P, Reddy MA, et al. Alpha-B Crystallin Gene (CRYAB) Mutation Causes Dominant Congenital Posterior Polar Cataract in Humans. *Am J Hum Genet*. 2001;69:1141–1145.
20. Bova MP, Yaron O, Huang Q, et al. Mutation R120G in alphaB-crystallin, which is linked to a desmin- related myopathy, results in an irregular structure and defective chaperone-like function. *Proc Natl Acad Sci USA*. 1999;96:6137–6142.
21. Vicart P, Caron A, Guicheney P, et al. A missense mutation in the αB-crystallin chaperone gene causes a desmin-related myopathy. *Nat Genet*. 1998;20:92–95.
22. Pras E, Frydman M, Levy-Nissenbaum E, et al. A nonsense mutation (W9X) in CRYAA causes autosomal recessive cataract in an inbred Jewish Persian family. *Invest Ophthalmol Vis Sci*. 2000;41:3511–3515.
23. Mackay DS, Boskovska OB, Knopf HL, Lampi KJ, Shiels A. A nonsense mutation in CRYBB1 associated with autosomal dominant cataract linked to human chromosome 22q. *Am J Hum Genet*. 2002;71:1216–1221.
24. Litt M, Carrero-Valenzuela R, LaMorticella DM, et al. Autosomal dominant cerulean cataract is associated with a chain termination mutation in the human beta-crystallin gene CRYBB2. *Hum Mol Genet*. 1997;6:665–668.
25. Gill D, Klose R, Munier FL, et al. Genetic heterogeneity of the Coppock-like cataract: a mutation in CRYBB2 on chromosome 22q11.2. *Invest Ophthalmol Vis Sci*. 2000;41:159–165.
26. Heon E, Priston M, Schorderet DF, et al. The gamma-crystallins and human cataracts: a puzzle made clearer. *Am J Hum Genet*. 1999;65:1261–1267.
27. Ren Z, Li A, Shastry BS, et al. A 5-base insertion in the γC-crystallin gene is associated with autosomal dominant variable zonular pulverulent cataract. *Hum Genet*. 2000;106:531–537.
28. Santhiya ST, Shyam MM, Rawlley D, et al. Novel mutations in the gamma-crystallin genes cause autosomal dominant congenital cataracts. *J Med Genet*. 2002;39:352–358.
29. Stephan DA, Gillanders E, Vanderveen D, et al. Progressive juvenile-onset punctate cataracts caused by mutation of the gammaD-crystallin gene. *Proc Natl Acad Sci USA*. 1999;96:1008–1012.
30. Kmoch S, Brynda J, Asfaw B, et al. Link between a novel human gammaD-crystallin allele and a unique cataract phenotype explained by protein crystallography. *Hum Mol Genet*. 2000;9:1779–1786.
31. Ren Z, Lin PY, Klintworth GK, et al. Allelic and locus heterogeneity in autosomal recessive gelatinous drop-like corneal dystrophy. *Hum Genet*. 2002;110:568–577.
32. Heon E, Priston MK, Billingsley G, Lubsen NH, Munier F. Clarifying the role of gamma-crystallin in congenital CCL cataract (abstract). *Am J Hum Genet*. 1999;65:A19.
33. Krivandin AV, Lvov YM, Ostrovski MA, Fedorovich IB, Feigin LA. Structural conversions of crystallins under senile cataract, dehydration and UV-irradiation studied by X-ray diffraction. *Exp Eye Res*. 1989;49:853–859.
34. Hott JL, Borkman RF. Concentration dependence of transmission losses in UV-laser irradiated bovine alpha-, beta H-, beta L- and gamma-crystallin solutions. *Photochem Photobiol*. 1993;57:312–317.
35. Li DY, Borkman RF, Wang RH, Dillon J. Mechanisms of photochemically produced turbidity in lens protein solutions. *Exp Eye Res*. 1990;51:663–669.
36. Borkman RF, Knight G, Obi B. The molecular chaperone alpha-crystallin inhibits UV-induced protein aggregation. *Exp Eye Res*. 1996;62:141–148.
37. Andley UP, Sawardekar MA, Burris JL. Action spectrum for photocross-linking of human lens proteins. *Photochem Photobiol*. 1997;65:556–559.
38. Ostrovsky MA, Sergeev YV, Atkinson DB, Soustov LV, Hejtmancik JF. Comparison of ultraviolet induced photo-kinetics for lens-derived and recombinant beta-crystallins. *Mol Vis*. 2002;8:72–78.
39. van Rens GL, de Jong WW, Bloemendal H. A superfamily in the mammalian eye lens: the beta/gamma-crystallins. *Mol Biol Rep*. 1992;16:1–10.
40. Hope JN, Chen H-C, Hejtmancik JF. Aggregation of betaA3-crystallin is independent of the specific sequence of the domain connecting peptide. *J Biol Chem*. 1994;269:21141–21145.
41. Hope JN, Chen HC, Hejtmancik JF. BetaA3/A1-crystallin association: role of the amino terminal arm. *Protein Eng*. 1994;7:445–451.
42. Laemmli UK. Cleavage of structural proteins during the assembly of the head of bacteriophage T4. *Nature*. 1970;227:680–685.
43. Davis MT, Stahl DC, Hefta SA, Lee TD. A microscale electrospray interface for on-line, capillary liquid chromatography/tandem mass spectrometry of complex peptide mixtures. *Anal Chem*. 1995;67:4549–4556.
44. Eng JK, McCormack AL, Yates JR III. An approach to correlate tandem mass spectral data of peptides with amino acid sequences in a protein database. *J Am Soc Mass Spectrom*. 1994;5:976–989.
45. Perkins DN, Pappin DJ, Creasy DM, Cottrell JS. Probability-based protein identification by searching sequence databases using mass spectrometry data. *Electrophoresis*. 1999;20:3551–3567.
46. Andley UP, Clark BA. Photoreactions of human lens monomeric crystallins. *Biochim Biophys Acta*. 1989;997:284–291.
47. Ferrini W, Schorderet DF, Othenin-Girard P, et al. CRYBA3/A1 gene mutation associated with suture-sparing autosomal dominant congenital nuclear cataract: a novel phenotype. *Invest Ophthalmol Vis Sci*. 2004;45:1436–1441.
48. Trinkl S, Glockshuber R, Jaenicke R. Dimerization of beta B2-crystallin: the role of the linker peptide and the N- and C-terminal extensions. *Protein Sci*. 1994;3:1392–1400.
49. Hibbard LB, Kirk NJ, Borkman RF. The in vitro photolysis of whole rat lenses using focused 290 nm laser radiation. *Exp Eye Res*. 1985;40:285–295.
50. Dean RT, Fu S, Stocker R, Davies MJ. Biochemistry and pathology of radical-mediated protein oxidation. *Biochem J*. 1997;324:1–18.
51. Wu K, Kojima M, Shui YB, Sasaki K, Hockwin O. In vitro UV-B effect on lens protein solutions. *Ophthalmic Res*. 1997;29:75–82.
52. Kessel L, Kalinin S, Soroka V, Larsen M, Johansson LB. Impact of UVR-A on whole human lenses, supernatants of buffered human lens homogenates, and purified argpyrimidine and 3-OH-kynurenine. *Acta Ophthalmol Scand*. 2005;83:221–227.
53. Dilley KJ. Loss of tryptophan associated with photo-polymerization and yellowing of proteins exposed to light over 300nm. *Biochem J*. 1973;133:821–826.
54. Chao CC, Ma YS, Stadtman ER. Modification of protein surface hydrophobicity and methionine oxidation by oxidative systems. *Proc Natl Acad Sci USA*. 1997;94:2969–2974.
55. Kantorow M, Hawse JR, Cowell TL, et al. Methionine sulfoxide reductase A is important for lens cell viability and resistance to oxidative stress. *Proc Natl Acad Sci USA*. 2004;101:9654–9659.
56. Shearer TR, Ma H, Fukiage C, Azuma M. Selenite nuclear cataract: review of the model. *Mol Vis.* 1997;3:8.
57. Hanson SR, Hasan A, Smith DL, Smith JB. The major in vivo modifications of the human water-insoluble lens crystallins are

disulfide bonds, deamidation, methionine oxidation and backbone cleavage. *Exp Eye Res*. 2000;71:195–207.

58. Ueda Y, Duncan MK, David LL. Lens proteomics: the accumulation of crystallin modifications in the mouse lens with age. *Invest Ophthalmol Vis Sci*. 2002;43:205–215.
59. Lampi KJ, Shih M, Ueda Y, Shearer TR, David LL. Lens proteomics: analysis of rat crystallin sequences and two-dimensional electrophoresis map. *Invest Ophthalmol Vis Sci*. 2002;43:216–224.
60. Taylor A. Associations between nutrition and cataract. *Nutr Rev*. 1989;47:225–234.
61. Zigman S. Environmental near-UV radiation and cataracts. *Optom Vis Sci*. 1995;72:899–901.
62. Reddy VN. Glutathione and its function in the lens: an overview. *Exp Eye Res*. 1990;50:771–778.
63. Spector A. The search for a solution to senile cataracts. Proctor Lecture. *Invest Ophthalmol Vis Sci*. 1984;25:130–146.